




Cite this: *RSC Adv.*, 2021, 11, 14148

# Structure transition of a C<sub>60</sub> monolayer on the Bi(111) surface

Ya-Ru Wang, Min-Long Tao, \* Ma Chao-Ke, Zi-Long Wang, Da-Xiao Yang, Ming-Xia Shi, Kai Sun, Ji-Yong Yang and Jun-Zhong Wang \*

The interfacial structures of C<sub>60</sub> molecules adsorbed on solid surfaces are essential for a wide range of scientific and technological processes in carbon-based nanodevices. Here, we report structural transitions of the C<sub>60</sub> monolayer on the Bi(111) surface studied *via* low-temperature scanning tunneling microscopy (STM). With an increase in temperature, the structure of the C<sub>60</sub> monolayer transforms from local-order structures to a ( $\sqrt{93} \times \sqrt{93}$ ) R20° superstructure, and then to a (11 × 11) R0° superstructure. Moreover, the individual C<sub>60</sub> molecules in different superstructures have different orientations. C<sub>60</sub> molecules adopt the 6 : 6 C–C bond and 5 : 6 C–C bond facing-up, mixed orientations, and hexagon facing-up in the local-order structure, ( $\sqrt{93} \times \sqrt{93}$ ) R20°, and (11 × 11) R0° superstructure, respectively. These results shed important light on the growth mechanism of C<sub>60</sub> molecules on solid surfaces.

Received 3rd February 2021  
Accepted 31st March 2021

DOI: 10.1039/d1ra00900a

rsc.li/rsc-advances

## Introduction

C<sub>60</sub> molecule, as a prototypical fullerene molecule, has attracted widespread attention due to its potential in endohedral fullerenes,<sup>1</sup> photovoltaic devices,<sup>2</sup> peapod nanotubes,<sup>3</sup> and single-molecule transistors.<sup>4</sup> A C<sub>60</sub> monolayer grown on solid surfaces is critical for understanding and controlling the interfacial properties of fullerene-derived electronic and photovoltaic devices.<sup>5,6</sup> STM studies demonstrated that the C<sub>60</sub> monolayer on the solid surface exhibit a variety of lattice orientations such as the “in phase” ( $2\sqrt{3} \times 2\sqrt{3}$ ) R30°, <sup>7–13</sup> ( $7 \times 7$ ) R0°<sup>13</sup> and ( $\sqrt{589} \times \sqrt{589}$ ) R14.5°. <sup>13–15</sup> The individual molecules of fullerene and fulleride within a single domain display different orientations. In the complex orientational ordering ( $7 \times 7$ ) R0° structure, a 7-molecule C<sub>60</sub> cluster consists of a central molecule sitting atop of a gold atom and six tilted surrounding molecules.<sup>10</sup> In the unit cell of the ( $\sqrt{589} \times \sqrt{589}$ ) R14.5° structure, 49 C<sub>60</sub> molecules adopt 11 different orientations.<sup>14</sup> In the ( $2\sqrt{3} \times 2\sqrt{3}$ ) R30° structure, all C<sub>60</sub> molecules are in the same orientation.<sup>12,16</sup> The complex chiral motifs have been observed.<sup>17</sup> In C<sub>sn</sub>C<sub>60</sub> fulleride films, orientational ordering appears.<sup>18</sup> Moreover, “bright” and “dim” molecules have been widely found in the C<sub>60</sub> monolayer.<sup>9–17</sup> However, the “dim” molecules in superstructures reported so far arrange irregularly.

The structure of C<sub>60</sub> monolayers grown on the solid surface is not only related to C<sub>60</sub> molecules themselves but also the substrate. In the past reports, there have been a large number of investigation on the C<sub>60</sub> monolayer structures grown on numerous metals or semiconducting substrates, such as

Ag,<sup>7–9,19,20</sup> Au,<sup>10–16,21,22</sup> Cu,<sup>23–25</sup> graphene,<sup>26,27</sup> Si,<sup>28,29</sup> Ge,<sup>30</sup> C<sub>60</sub>,<sup>29</sup> or NaCl.<sup>31</sup> However, few reports address the superstructure of C<sub>60</sub> molecules adsorbed on semi-metal substrates. It is found that thin films of organic molecules grown on a semi-metallic Bi(111) surface shows a lot of interesting phenomena, such as the ordered crystalline layer with the standing-up orientation of pentacene molecules,<sup>32</sup> the chiral self-assembly of rubrene molecules,<sup>33</sup> structural transitions in different monolayers of cobalt phthalocyanine films,<sup>34</sup> and the Moiré’ pattern in C<sub>60</sub> thin films.<sup>35</sup>

In this study, we use Bi(111) as the substrate and studied the structure transition of the C<sub>60</sub> monolayer. C<sub>60</sub> molecules were deposited at 100 K form local-order structures. When the deposition temperature increased to room temperature, the local-order structures turn into a long-range ordered ( $\sqrt{93} \times \sqrt{93}$ ) R20° superstructure. After annealing at 400 K, the ordered superstructure transforms into the (11 × 11) R0° superstructure. These superstructures are different from the structures of the C<sub>60</sub> monolayer reported so far. Furthermore, the individual C<sub>60</sub> molecules in the local-order structure, ( $\sqrt{93} \times \sqrt{93}$ ) R20° and (11 × 11) R0° superstructure, show the 6 : 6 C–C bond and 5 : 6 C–C bond facing-up, mixed orientations, and hexagon facing-up, respectively. The 6 : 6 (5 : 6) C–C bond indicates the common side of two adjacent hexagons (pentagon and hexagon) in C<sub>60</sub> molecules.

## Experimental

The experiments were conducted in an ultra-high vacuum low-temperature scanning tunneling microscope produced by Uni-soku. The base pressure was kept at  $\sim 1.2 \times 10^{-10}$  Torr. An Si(111) substrate was continuously degassed at  $\sim 870$  K for 8 h

School of Physical Science and Technology, Southwest University, Chongqing, China.  
E-mail: taotaole@swu.edu.cn; jzwangcn@swu.edu.cn



with subsequent flashing to 1400 K for several seconds. The Bi(111) film was prepared by depositing 20 monolayers of bismuth atoms on a Si(111)- $7 \times 7$  surface at room temperature with subsequent annealing at 400 K.<sup>36</sup> C<sub>60</sub> molecules were deposited onto the Bi(111) surface by heating the tantalum cell to 700 K. The growth rate of C<sub>60</sub> molecules was about 0.4 monolayers per minute. All STM images were acquired with a tungsten tip in constant-current mode at liquid nitrogen temperature (78 K).

## Results and discussion

First, a small number of C<sub>60</sub> molecules were deposited onto the Bi(111) surface when the substrate was maintained at 100 K. Fig. 1(a) shows the atomic-resolution image of the hexagonal lattices of the Bi(111) thin film. The lattice constants of the Bi(111) surface are measured to be  $a_1 = a_2 = 0.45 \pm 0.02$  nm, very close to the bulk value ( $a = 0.454$  nm) in Bi crystals.<sup>36</sup> Fig. 1(b) shows the isolated C<sub>60</sub> molecules on the Bi(111) surface presenting round protrusions. When reducing the bias voltage, the round protrusions are separated into two asymmetrical [Fig. 1(c)] or symmetrical [Fig. 1(d)] lobes, corresponding to the two different adsorption configurations, 5 : 6 C–C bond facing-up and 6 : 6 C–C bond facing-up, similar to C<sub>60</sub> molecules on Au(111).<sup>12</sup> This indicates that there are two stable adsorption orientations of isolated C<sub>60</sub> molecules on the Bi(111) substrate, 6 : 6 C–C bond, and 5 : 6 C–C bond facing-up.

When the coverage increases, C<sub>60</sub> molecules form the close-packed hexagonal structure, as shown in Fig. 2. We noticed that all the C<sub>60</sub> molecules present a uniform height, except a few dim molecules (marked by green dotted circles). The brightness contrast in images stems from the different adsorption sites of C<sub>60</sub> molecules. It is well known that metal surfaces do not behave as rigid templates for the chemisorption of C<sub>60</sub> molecules, but may reconstruct substantially to accommodate the molecules.<sup>37</sup> We speculate that Dim C<sub>60</sub> molecules are located at

the vacancies of the Bi(111) substrate, originating from the reconstruction of the Bi(111) surface, similar to C<sub>60</sub> molecules on Au(111)<sup>16</sup> and Cu(111).<sup>38</sup>

According to the arrangement of bright and dim molecules, we can see some local-order structures, though there is a lack of long-range ordering. In Fig. 2(a), there is an  $(11 \times 8)$  R0° local-order structure (marked by red parallelogram). The lattice directions of  $(11 \times 8)$  R0° are along with the directions of Bi(111), and the measured lattice constants are  $5.00 \pm 0.02$  nm and  $3.64 \pm 0.02$  nm, corresponding to 11 and 8 times of the lattice constant of the Bi(111) surface. The lattice directions of Bi(111) were obtained on the surface, which was not covered with C<sub>60</sub> molecules. In another domain, shown in Fig. 2(b), the local-order structure is mixed with three types of structures, namely  $(11 \times 8)$  R0° (red quadrilateral),  $(11 \times 11)$  R0° (white quadrilateral), and  $(10 \times 8)$  R10° (blue quadrilateral). In particular, we noticed that C<sub>60</sub> molecules exhibit almost the same orientation in a single domain, and most of the individual C<sub>60</sub> molecules in the local-order structure adopt two favorite orientations (6 : 6 C–C bond and 5 : 6 C–C bond facing up) as the isolated molecules on Bi(111). For example, most of the molecules shown in Fig. 2(a) present two symmetrical lobes, corresponding to C<sub>60</sub> molecules with a 6 : 6 C–C bond facing up. However, in Fig. 2(b), the molecules present two asymmetric lobes, corresponding to the 5 : 6 C–C bond facing up. We suggest that the formation of a local-order structure is due to the low-temperature growth. Because of the low kinetic energy of C<sub>60</sub> molecules at 100 K, molecular mobility is not high enough to form a long-range ordered superstructure. The C<sub>60</sub> molecules adsorbed on Bi(111) adopt their preferred orientations (6 : 6 C–C bond and 5 : 6 C–C bond facing up), similar to the isolated molecules adsorbed on the substrate. This proves the strong molecule–substrate interaction in the local-order structure.

To investigate the influence of temperature on the structure, we deposited C<sub>60</sub> molecules on Bi(111) at room temperature. It

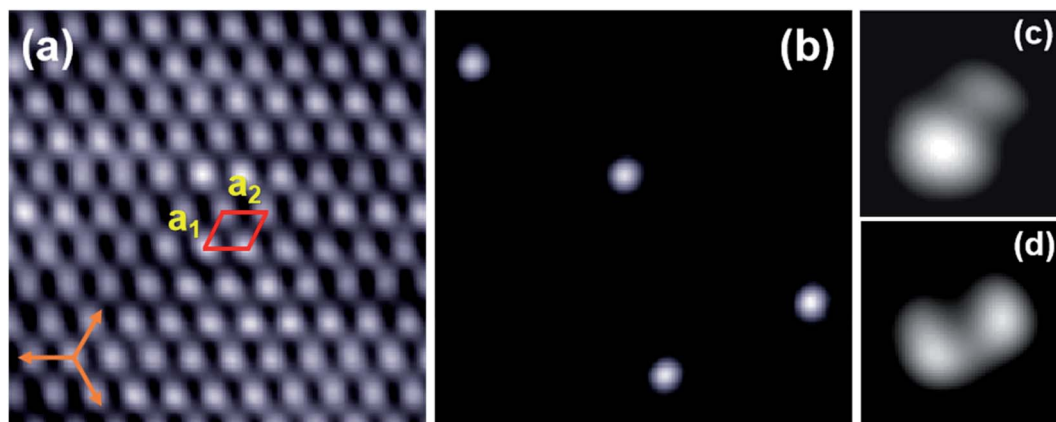


**Fig. 1** The initial stage of C<sub>60</sub> molecules adsorbed on the Bi(111) surface. (a) Hexagonal lattices of the Bi(111) surface, 5 nm  $\times$  5 nm,  $-0.1$  V. The unit cell is marked with a red box and the orange arrows indicate the directions of the Si(111) substrate. (b) Isolated C<sub>60</sub> molecules adsorbed on Bi(111), 20 nm  $\times$  20 nm, 2.2 V. (c) STM image of an isolated C<sub>60</sub> molecule with two asymmetrical lobes corresponding to the 5 : 6 C–C bond facing up, 1.3 nm  $\times$  1.3 nm, 400 mV. (d) STM image of an isolated C<sub>60</sub> molecule with two symmetrical lobes corresponding to the 6 : 6 C–C bond facing up, 1.3 nm  $\times$  1.3 nm, 200 mV.



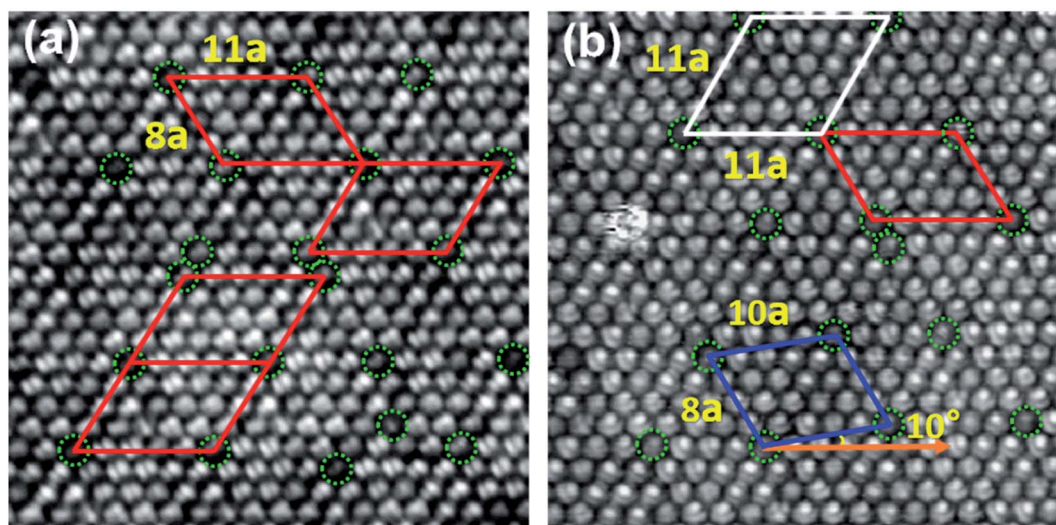


Fig. 2 Local-order structure in the monolayer  $C_{60}$  grown at a low temperature ( $\sim 100$  K). (a) Four unit cells of the  $(11 \times 8)$   $R0^\circ$  superstructure appeared in the  $C_{60}$  monolayer,  $20 \text{ nm} \times 20 \text{ nm}$ ,  $-1.2 \text{ V}$ . The dim  $C_{60}$  molecules, located at the hollow position of Bi(111), are marked by the green dotted circles. (b) The mixture of three types of superstructures,  $20 \text{ nm} \times 20 \text{ nm}$ ,  $-0.9 \text{ V}$ . The red, white, and blue unit cells correspond to the superstructure  $(11 \times 8)$   $R0^\circ$ ,  $(11 \times 11)$   $R0^\circ$ , and  $(10 \times 8)$   $R10^\circ$ .

is found that  $C_{60}$  molecules aggregate into a hexagonal structure, the same as  $C_{60}$  molecules in the local-order structure. However, the local-order structures, originating from the dim and bright molecules, turn into a long-range ordered  $(\sqrt{93} \times \sqrt{93})$   $R20^\circ$  superstructure [Fig. 3(a)]. This superstructure is different from the structures of the  $C_{60}$  monolayer reported so far. There is a misorientation angle of  $20^\circ$  between the lattice directions of the  $C_{60}$  monolayer and the Bi(111) surface. The measured lattice constants of  $(\sqrt{93} \times \sqrt{93})$   $R20^\circ$  are  $b_1 = b_2 = 4.38 \pm 0.02 \text{ nm}$ , agreeing well with  $\sqrt{93}$  times the lattice constant of Bi(111) ( $0.45 \text{ nm}$ ). Fig. 3(b) shows the schematic of the  $(\sqrt{93} \times \sqrt{93})$   $R20^\circ$  superstructure. Based on the lattice constant of the Bi(111) substrate, the lattice vectors of the  $(\sqrt{93} \times \sqrt{93})$   $R20^\circ$  superstructure can be expressed as following matrices:

$$\begin{pmatrix} b_1 \\ b_2 \end{pmatrix} = \begin{pmatrix} 11 & -4 \\ 4 & 7 \end{pmatrix} \begin{pmatrix} a_1 \\ a_2 \end{pmatrix}$$

This ordered superstructure implies two things: first, the intermolecular interaction is getting stronger than that in the local-order structure prepared at low temperature ( $100 \text{ K}$ ). Second, the molecule–substrate interaction is also strong since the orientations of the  $C_{60}$  superstructure are commensurate with those of the substrate. Furthermore, we can clearly see that individual  $C_{60}$  molecules adopt various orientations, rather than the favorite orientations as  $C_{60}$  molecules in the local-order structure. As shown in the high-resolution STM image [Fig. 3(c)],  $C_{60}$  molecules in  $(\sqrt{93} \times \sqrt{93})$   $R20^\circ$  present various shapes, such as two asymmetric lobes (white circle), two symmetrical lobes (yellow circle), and three lobes (blue circle),

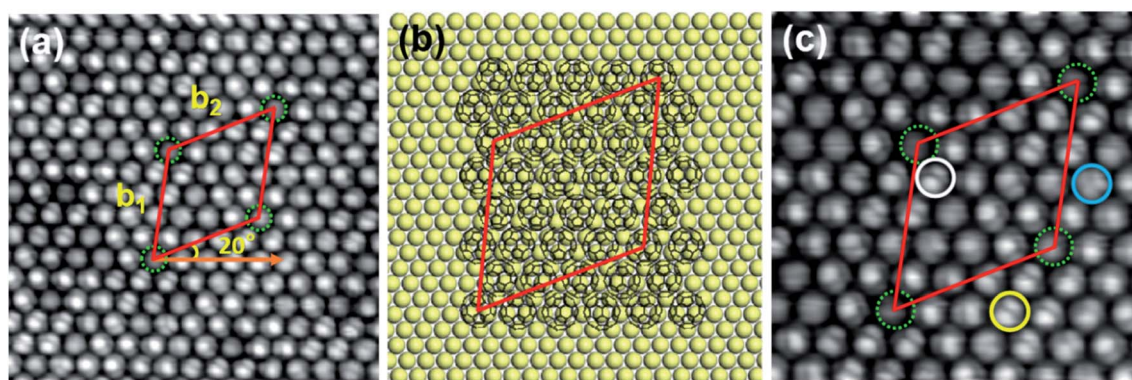


Fig. 3 (a) The STM image of the  $(\sqrt{93} \times \sqrt{93})$   $R20^\circ$  superstructure,  $15 \text{ nm} \times 15 \text{ nm}$ ,  $-1.2 \text{ V}$ . (b) Schematic model of the  $(\sqrt{93} \times \sqrt{93})$   $R20^\circ$  superstructure. The yellow balls and black hollow balls represent Bi atoms and  $C_{60}$  molecules. (c) High-resolution STM image of the  $(\sqrt{93} \times \sqrt{93})$   $R20^\circ$  superstructure,  $10 \text{ nm} \times 10 \text{ nm}$ ,  $-1.0 \text{ V}$ . The individual molecules exhibit different orientations, such as 5 : 6 C–C bond, 6 : 6 C–C bond, and hexagon facing up, marked by white, yellow, and blue solid circles, respectively.





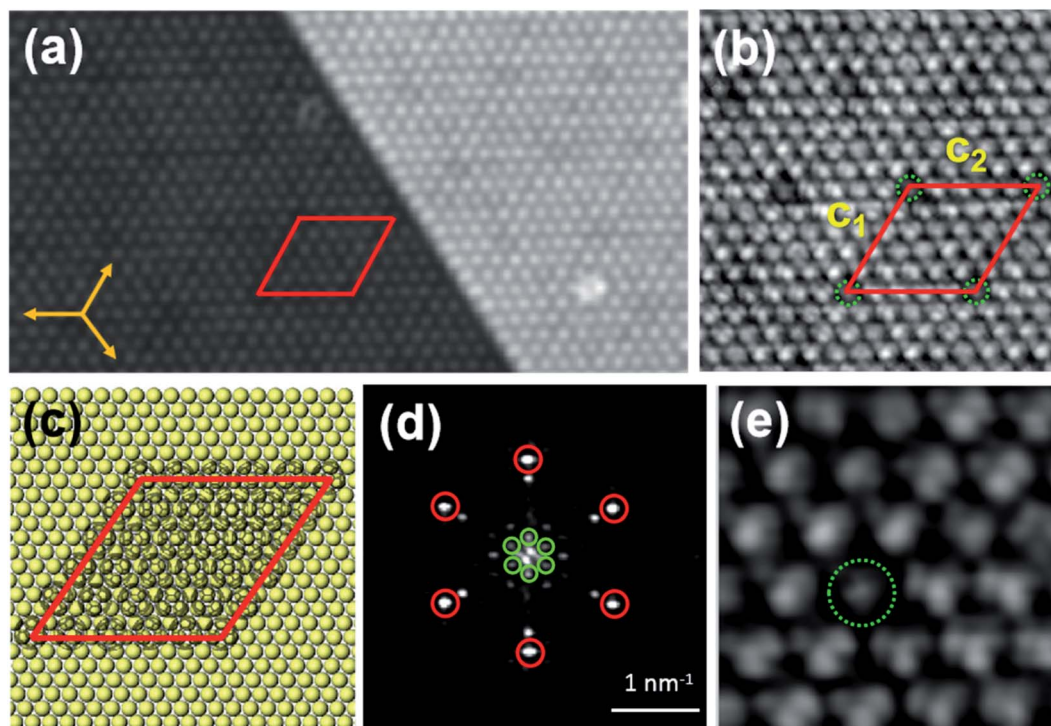


Fig. 4 (a) The STM image of the  $(11 \times 11)$   $R0^\circ$  superstructure corresponding to the Bi(111),  $39 \text{ nm} \times 21 \text{ nm}$ ,  $-1.5 \text{ V}$ . (b) Close-up view of the  $(11 \times 11)$   $R0^\circ$  superstructure,  $14 \text{ nm} \times 14 \text{ nm}$ ,  $-0.7 \text{ V}$ . (c) Schematic model of the  $(11 \times 11)$   $R0^\circ$  superstructure with respect to the Bi(111) lattices. (d) FFT of the image (a). The spots marked by red circles correspond to the  $C_{60}$  hexagonal lattices, while the spots marked by the green circles represent the  $(11 \times 11)$   $R0^\circ$  superstructure. (e) STM image with a sub-molecular resolution of the superstructure,  $5 \text{ nm} \times 5 \text{ nm}$ ,  $-0.7 \text{ V}$ .

corresponding to the  $5:6$  C–C bond,  $6:6$  C–C bond, and hexagon facing up. The diversity of  $C_{60}$  molecular orientations is due to the enhancement of intermolecular interaction in the  $(\sqrt{93} \times \sqrt{93})$   $R20^\circ$  superstructure. The intermolecular interaction enables  $C_{60}$  molecules to overcome the molecule–substrate interaction and adopt other orientations, and then make the  $(\sqrt{93} \times \sqrt{93})$   $R20^\circ$  superstructure stable.

When annealed at  $400 \text{ K}$  for about  $20 \text{ min}$ ,  $C_{60}$  molecules still revealed a hexagonal lattice, while the superstructure transformed from  $(\sqrt{93} \times \sqrt{93})$   $R20^\circ$  into  $(11 \times 11)$   $R0^\circ$  superstructure [Fig. 4(a)], indicating that  $(11 \times 11)$   $R0^\circ$  is more stable than  $(\sqrt{93} \times \sqrt{93})$   $R20^\circ$ . The lattice directions of  $(11 \times 11)$   $R0^\circ$  are along the directions of the Bi(111) substrate, and the lattice constants are  $c_1 = c_2 = 5.00 \pm 0.02 \text{ nm}$  [Fig. 4(b)], corresponding to 11 times of the lattice constant of Bi(111). Fig. 4(d) is the fast Fourier transform (FFT) image of the  $(11 \times 11)$   $R0^\circ$  superstructure, where the spots marked by red and green circles correspond to  $C_{60}$  hexagonal lattices and the  $(11 \times 11)$   $R0^\circ$  superstructure. In the FFT image, the spots of the superstructure are clearly visible, though they are dimmer than the spots of  $C_{60}$  hexagonal lattices, implying that the  $(11 \times 11)$   $R0^\circ$  superstructure has long-range order. The schematic model of  $(11 \times 11)$   $R0^\circ$  is shown in Fig. 4(c). From STM images, the  $(11 \times 11)$   $R0^\circ$  superstructure seems to have the same structure as the reported structure attributed to a Moiré' pattern in ref. 36. However, in our experiment, the  $(11 \times 11)$   $R0^\circ$  superstructure is transformed from the  $(\sqrt{93} \times \sqrt{93})$   $R20^\circ$  superstructure and

have no relationship with the Moiré' pattern. From the close-up view of the  $(11 \times 11)$   $R0^\circ$  superstructure in Fig. 4(e), it is found that all the  $C_{60}$  molecules reveal a unified three-lobe structure, corresponding to the hexagon facing up, different from favorite orientations in the local-order structure and mixed orientations in  $(\sqrt{93} \times \sqrt{93})$   $R20^\circ$ . With an increase in temperature, the superstructure of the  $C_{60}$  monolayer changes from local order to long-range order and  $C_{60}$  molecules are re-orientated. This is because the thermal diffusivities of  $C_{60}$  molecules and Bi atoms increase with the increase in temperature, which is conducive to the formation of a more orderly and stable superstructure.

## Conclusions

In summary, the structure of  $C_{60}$  molecules on Bi(111) changes with temperature variation. When deposited on the Bi(111) surface at  $100 \text{ K}$ ,  $C_{60}$  molecules form local-order structures, and the molecules in local-order structures adopt their favorite orientations. As the deposition temperature increases to room temperature, the local-order structures turn into a long-range ordered  $(\sqrt{93} \times \sqrt{93})$   $R20^\circ$  superstructure. The orientations of  $C_{60}$  molecules in  $(\sqrt{93} \times \sqrt{93})$   $R20^\circ$  superstructures are diverse. After annealing at  $400 \text{ K}$  for about  $20 \text{ min}$ , the  $C_{60}$  film exhibits a  $(11 \times 11)$   $R0^\circ$  superstructure, and all  $C_{60}$  molecules in this superstructure take the unified orientation, hexagon facing-up. The appearance of numerous superstructures and the molecular orientations in superstructures is due to the change in the



thermal diffusivity of C<sub>60</sub> molecules and Bi atoms at different temperatures.

## Conflicts of interest

There are no conflicts to declare.

## Acknowledgements

This work was supported by the National Natural Science Foundation of China (Grant Nos. 11804282, 11874304, 11574253).

## References

- 1 T. Ohtsuki, K. Masumoto, K. Ohno, Y. Maruyama, Y. Kawazoe, K. Sueki and K. Kikuchi, Insertion of Be Atoms in C<sub>60</sub> Fullerene Cages: Be@C<sub>60</sub>, *Phys. Rev. Lett.*, 1996, **77**, 3522.
- 2 C. Deibel and V. Dyakonov, Polymer–fullerene bulk heterojunction solar cells, *Rep. Prog. Phys.*, 2010, **73**, 096401.
- 3 D. J. Hornbaker, S.-J. Kahng, S. Misra, B. W. Smith, A. T. Johnson, E. J. Mele, D. E. Luzzi and A. Yazdani, Mapping the One-Dimensional Electronic States of Nanotube Peapod Structures, *Science*, 2002, **295**, 828–831.
- 4 H. Park, J. Park, A. K. L. Lim, E. H. Anderson, A. P. Alivisatos and P. L. McEuen, Nanomechanical oscillations in a single-C<sub>60</sub> transistor, *Nature*, 2000, **407**, 57–60.
- 5 P. W. Stephens, G. Bortel, G. Faigel, M. Tegze, A. Jánosy, S. Pekker, G. Oszlanyi and L. Forró, Polymeric fullerene chains in RbC<sub>60</sub> and KC<sub>60</sub>, *Nature*, 1994, **370**, 636–639.
- 6 R. Yamachika, M. Grobis, A. Wachowiak and M. F. Crommie, Controlled atomic doping of a single molecule, *Science*, 2004, **304**, 281–284.
- 7 H. I. Li, K. Pussi, K. J. Hanna, L. L. Wang, D. D. Johnson, H. P. Cheng, H. Shin, S. Curtarolo, W. Moritz and J. A. Smerdon, Surface Geometry of C<sub>60</sub> on Ag(111), *Phys. Rev. Lett.*, 2009, **103**, 056101.
- 8 K. Pussi, H. I. Li, H. Shin, L. N. S. Loli, A. K. Shukla, J. Ledieu, V. Fournée, L. L. Wang, S. Y. Su and K. E. Marino, Elucidating the dynamical equilibrium of C<sub>60</sub> molecules on Ag(111), *Phys. Rev. B: Condens. Matter Mater. Phys.*, 2012, **86**, 205426.
- 9 H. I. Li, G. J. P. Abreu, A. K. Shukla, V. Fournée, J. Ledieu, L. N. Serkovic Loli, S. E. Rauterkus, M. V. Snyder, S. Y. Su and K. E. Marino, Ordering and dynamical properties of superbright C<sub>60</sub> molecules on Ag(111), *Phys. Rev. B: Condens. Matter Mater. Phys.*, 2014, **89**, 085428.
- 10 L. Tang, Y. Xie and Q. Guo, Complex orientational ordering of C<sub>60</sub> molecules on Au(111), *J. Chem. Phys.*, 2011, **135**, 11470211.
- 11 X. Torrelles, M. Pedio, C. Cepek and R. Felici, (2√3 × 2√3) R30 degrees induced self-assembly ordering by C<sub>60</sub> on a Au(111) surface: X-ray diffraction structure analysis, *Phys. Rev. B: Condens. Matter Mater. Phys.*, 2012, **86**, 075461.
- 12 M. Passens, R. Waser and S. Karthaeuser, Enhanced fullerene-Au(111) coupling in (2√3 × 2√3)R30 degrees superstructures with intermolecular interactions, *Beilstein J. Nanotechnol.*, 2015, **6**, 1421–1431.
- 13 H. Shin, A. Schwarze, R. D. Diehl, K. Pussi, A. Colombier, E. Gaudry, J. Ledieu, G. M. McGuirk, L. N. S. Loli and V. Fournée, Structure and dynamics of C<sub>60</sub> molecules on Au(111), *Phys. Rev. B: Condens. Matter Mater. Phys.*, 2014, **89**, 245428.
- 14 G. Schull and R. Berndt, Orientationally ordered (7 × 7) superstructure of C<sub>60</sub> on Au(111), *Phys. Rev. Lett.*, 2007, **99**, 226105.
- 15 X. Zhang, F. Yin, R. E. Palmer and Q. Guo, The C<sub>60</sub>/Au(111) interface at room temperature: A scanning tunnelling microscopy study, *Surf. Sci.*, 2008, **602**, 885–892.
- 16 J. A. Gardener, G. A. D. Briggs and M. R. Castell, Scanning tunneling microscopy studies of C<sub>60</sub> monolayers on Au(111), *Phys. Rev. B: Condens. Matter Mater. Phys.*, 2009, **80**, 235434.
- 17 Y. Z. Shang, Z. L. Wang, D. X. Yang, Y. Y. Wang, C. K. Ma, M. L. Tao, K. Sun, J. Y. Yang and J. Z. Wang, Orientation ordering and chiral superstructures in fullerene monolayer on Cd(0001), *Nanomaterials*, 2020, **10**, 1305.
- 18 S. Han, M. X. Guan, C. L. Song, Y. L. Wang, M. Q. Ren, S. Meng, X. C. Ma and Q. K. Xue, Visualizing molecular orientational ordering and electronic structure in CsnC<sub>60</sub> fulleride films, *Phys. Rev. B*, 2020, **101**, 085413.
- 19 W. W. Pai and C. L. Hsu, Ordering of an incommensurate molecular layer with adsorbate-induced reconstruction: C<sub>60</sub>/Ag(100), *Phys. Rev. B: Condens. Matter Mater. Phys.*, 2003, **68**, 121403.
- 20 C. Grosse, O. Gunnarsson, P. Merino, K. Kuhnke and K. Kern, Nanoscale Imaging of Charge Carrier and Exciton Trapping at Structural Defects in Organic Semiconductors, *Nano Lett.*, 2016, **16**, 2084–2089.
- 21 L. Tang, X. Zhang, Q. Guo, Y. Wu, L. Wang and H. Cheng, Two bonding configurations for individually adsorbed C<sub>60</sub> molecules on Au(111), *Phys. Rev. B: Condens. Matter Mater. Phys.*, 2010, **82**, 125414.
- 22 L. Tang, X. Zhang and Q. Guo, Organizing C<sub>60</sub> molecules on a nanostructured Au(111) surface, *Surf. Sci.*, 2010, **604**, 1310–1314.
- 23 T. Hashizume, K. Motai, X. D. Wang, H. Shinohara, Y. Saito, Y. Maruyama, K. Ohno, Y. Kawazoe, Y. Nishina and H. W. Pickering, Intramolecular structures of C<sub>60</sub> molecules adsorbed on the Cu(111)-(1 × 1) surface, *Phys. Rev. Lett.*, 1993, **71**, 2959–2962.
- 24 S. Wong, W. W. Pai, C. Chen and M. Lin, Coverage-dependent adsorption superstructure transition of C<sub>60</sub>/Cu(001), *Phys. Rev. B: Condens. Matter Mater. Phys.*, 2010, **82**, 125442.
- 25 G. Xu, X. Shi, R. Q. Zhang, W. W. Pai, H. T. Jeng and M. A. Van Hove, Detailed low-energy electron diffraction analysis of the (4 × 4) surface structure of C<sub>60</sub> on Cu(111): Seven-atom-vacancy reconstruction, *Phys. Rev. B: Condens. Matter Mater. Phys.*, 2012, **86**, 075419.
- 26 G. Li, H. T. Zhou, L. D. Pan, Y. Zhang, J. H. Mao, Q. Zou, H. M. Guo, Y. L. Wang, S. X. Du and H. J. Gao, Self-assembly of C<sub>60</sub> monolayer on epitaxially grown, nanostructured graphene on Ru(0001) surface, *Appl. Phys. Lett.*, 2012, **100**, 0133041.



- 27 M. Jung, D. Shin, S. Sohn, S. Kwon, N. Park and H. Shin, Atomically resolved orientational ordering of C<sub>60</sub> molecules on epitaxial graphene on Cu(111), *Nanoscale*, 2014, **6**, 11835–11840.
- 28 J. G. Hou, J. L. Yang, H. Q. Wang, Q. X. Li, C. G. Zeng, H. Lin, W. Bing, D. M. Chen and Q. S. Zhu, Identifying molecular orientation of individual C<sub>60</sub> on a Si(111)-(7 × 7) surface, *Phys. Rev. Lett.*, 1999, **83**, 3001–3004.
- 29 H. Q. Wang, C. G. Zeng, B. Wang, J. G. Hou, Q. X. Li and J. L. Yang, Orientational configurations of the C<sub>60</sub> molecules in the (2 × 2) superlattice on a solid C<sub>60</sub> (111) surface at low temperature, *Phys. Rev. B: Condens. Matter Mater. Phys.*, 2001, **63**, 085417.
- 30 A. Goldoni, C. Cepek, M. De Seta, J. Avila, M. C. Asensio and M. Sancrotti, Interaction of C<sub>60</sub> with Ge(111) in the 3√3 × 3√3 R30° phase: A (2 × 2) model, *Phys. Rev. B: Condens. Matter Mater. Phys.*, 2000, **61**, 10411–10416.
- 31 J. Leaf, A. Stannard, S. P. Jarvis, P. Moriarty and J. L. Dunn, A combined monte carlo and huckel theory simulation of orientational ordering in C<sub>60</sub> assemblies, *J. Phys. Chem. C*, 2016, **120**, 8139–8147.
- 32 G. E. Thayer, J. T. Sadowski, F. M. z. Heringdorf, T. Sakurai and R. M. Tromp, Role of surface electronic structure in thin film molecular ordering, *Phys. Rev. Lett.*, 2005, **95**, 25610.
- 33 K. Sun, M. Lan and J. Z. Wang, Absolute configuration and chiral self-assembly of rubrene on Bi(111), *Phys. Chem. Chem. Phys.*, 2015, **17**, 26220.
- 34 M. L. Tao, Y. B. Tu, K. Sun, Y. Zhang, X. Zhang, Z. B. Li, S. J. Hao, H. F. Xiao, J. Ye and J. Z. Wang, Structural transitions in different monolayers of cobalt phthalocyanine film grown on Bi(111), *J. Phys. D: Appl. Phys.*, 2016, **49**, 015307.
- 35 J. T. Sadowski, R. Z. Bakhtizin, A. I. Oreshkin, T. Nishihara, A. Al-Mahboob, Y. Fujikawa, K. Nakajima and T. Sakurai, Epitaxial C<sub>60</sub> thin films on Bi(0001), *Surf. Sci.*, 2007, **601**, 136–139.
- 36 T. Nagao, J. T. Sadowski, M. Saito, S. Yaginuma, Y. Fujikawa, T. Kogure, T. Ohno, Y. Hasegawa, S. Hasegawa and T. Sakurai, Nanofilm allotrope and phase transformation of ultrathin Bi film on Si(111)-7 × 7, *Phys. Rev. Lett.*, 2004, **93**, 105501.
- 37 X. Q. Shi, A. M. Van Hove and R. Q. Zhang, Survey of structural and electronic properties of C<sub>60</sub> on close-packed metal surfaces, *J. Mater. Sci.*, 2012, **47**, 7341–7355.
- 38 W. W. Pai, H. T. Jeng, C. M. Cheng, C. H. Lin, X. Xiao, A. Zhao, X. Zhang, G. Xu, X. Q. Shi, M. A. Van Hove, C. S. Hsue and K. D. Tsuei, Optimal electron doping of a C<sub>60</sub> monolayer on Cu(111) via interface reconstruction, *Phys. Rev. Lett.*, 2010, **104**, 036103.

